The absorption spectrum of nitrous oxide between 7250 and 7653 cm–1

E.V. Karlovets, Didier Mondelain, S.A. Tashkun, A. Campargue

The absorption spectrum of nitrous oxide between 7250 and 7653 cm^{-1}

E.V. Karlovets [1,2*], D. Mondelain [1], S.A. Tashkun [3] and A. Campargue [1*]

[1] *Univ. Grenoble Alpes, CNRS, LIPhy, 38000 Grenoble, France*
[2] *Tomsk State University, Department of Optics and Spectroscopy, 36, Lenin Avenue, 634050, Tomsk, Russia*
[3] *V.E. Zuev Institute of Atmospheric Optics, 1, Academician Zuev square, 634055 Tomsk, Russia*

Number of pages: 26 19 October 2023

Number of tables: 3

Number of figures: 10

Keywords: Nitrous oxide, N_2O, high-resolution spectra, cavity ring down spectroscopy, line positions, line intensities, NOSL-296

* Corresponding author:
E-mail: alain.campargue@univ-grenoble-alpes.fr (A. Campargue)

Abstract

We revisit the weak absorption spectrum of natural nitrous oxide between 7250 and 7653 cm^{-1} for which rovibrational assignments were previously reported in Lu et al. (doi:10.1016/j.jqsrt.2012.03.005). Our main goal is to provide intensity information for the high number of lines detected by cavity ring down spectroscopy in the region. Line parameters of about 4180 transitions were retrieved from a line-by-line profile adjustment. They belong to 69 bands of the $^{14}N_2{}^{16}O$, $^{14}N^{15}N^{16}O$, $^{15}N^{14}N^{16}O$, and $^{14}N_2{}^{18}O$ isotopologues, present in natural isotopic abundance in the sample. Eight bands are newly reported. The band-by-band analysis allowed for the determination of refined values of the rovibrational parameters of a total of 68 upper vibrational states. Eight $^{14}N_2{}^{16}O$ bands were found affected by local rovibrational perturbations and a total of 31 extra lines due to an intensity transfer could be identified. The comparison with the recent NOSL-296 and Ames line lists is discussed in detail. The overall agreement is very satisfactory. As concerns line intensities, the NOSL and Ames lists show both specific advantages and drawbacks which are discussed.

1. Introduction

The present study is part of a long-term project aiming at characterizing the high sensitivity absorption spectrum of nitrous oxide in the near-infrared by cavity ring down spectroscopy (CRDS). **Fig. 1** presents an overview of our preceding studies [1-12] which cover continuously the 5696-8630 cm^{-1} range. The HITRAN2020 list [13] and the very recent Nitrous Oxide Spectroscopic line list (NOSL-296) (NOSL) [14] of $^{14}N_2{}^{16}O$ are included in the plot. The present version of the HITRAN list is mostly based on the SISAM.N2O line list constructed by Toth from spectra measured by Fourier transform spectroscopy (FTS) [15]. Most of the SISAM line positions and line intensities are calculated values obtained using spectroscopic parameters obtained from a band-by-band fit of line positions and line intensities. The SISAM list covers the 500-7800 cm^{-1} spectral range and includes transitions with line strength larger than about 2×10^{-25} cm/molecule at 296 K. The very recent NOSL-296 list [14] is a calculated line list with positions obtained using an effective Hamiltonian (EH) model with parameters fitted on experimental positions and intensities computed from effective dipole moments (EDM) with parameters fitted on measured line intensities. The NOSL-296 intensity cut off is 1×10^{-30} cm/molecule at 296 K, about five orders of magnitude lower than the HITRAN intensity threshold. Our previous CRDS studies [1-12] provided a large number of new line positions which were valuable to refine the parameters of the EH model. As concerns line intensity calculations, they require a set of EDM parameters for each ΔP value ($P= 2V_1+V_2+4V_3$ is the polyad number where $V_{i=1-3}$ are the vibrational quantum numbers). The sensitivity of our CRDS setup allows for the detection of lines with intensity on the order of 1×10^{-29} cm/molecule at 296 K which were valuable to fit the necessary EDM parameters [15]. We have highlighted in **Fig. 1** (red and blue open circles), the transitions for which line intensities were previously retrieved from the CRDS spectra. As illustrated by this figure, line intensities were reported for only part of the recorded CRDS spectra which makes some sets of EDM parameters inaccurate or incomplete.

In the present work, we reconsider the 7250 - 7653 cm^{-1} interval, first assigned by Lu et al. [5] in 2012. Intensity information was retrieved in Ref. [6] for about 740 lines of six strong bands measured at 2 Torr and 10 Torr in the region, which allowed fitting the dominant EDM parameters. Note that due to the relative weakness of the absorption in the region, (line intensities are smaller than 2×10^{-25} cm/molecule), no transitions are included in the HITRAN database in the considered interval. Here, using the same spectra as in Refs. [5,6], line intensities were systematically retrieved using a multiline fitting program for about 4180 transitions presented on the upper panel of **Fig. 1**. The resulting experimental list combined with improved predictions of the N_2O absorption spectrum will allow for:

i. the rovibrational assignment of a few additional bands not reported in Ref. [5],

ii. detailed analysis of some local rovibrational interactions leading to the detection of extra lines resulting from an intensity transfer,

iii. validation tests of the NOSL-296 list of $^{14}N_2{}^{16}O$ and the Ames line list for all the isotopologues, in particular, for the intensities of the weak bands. Deviations compared to NOSL intensities will help to refine the set of EDM parameters.

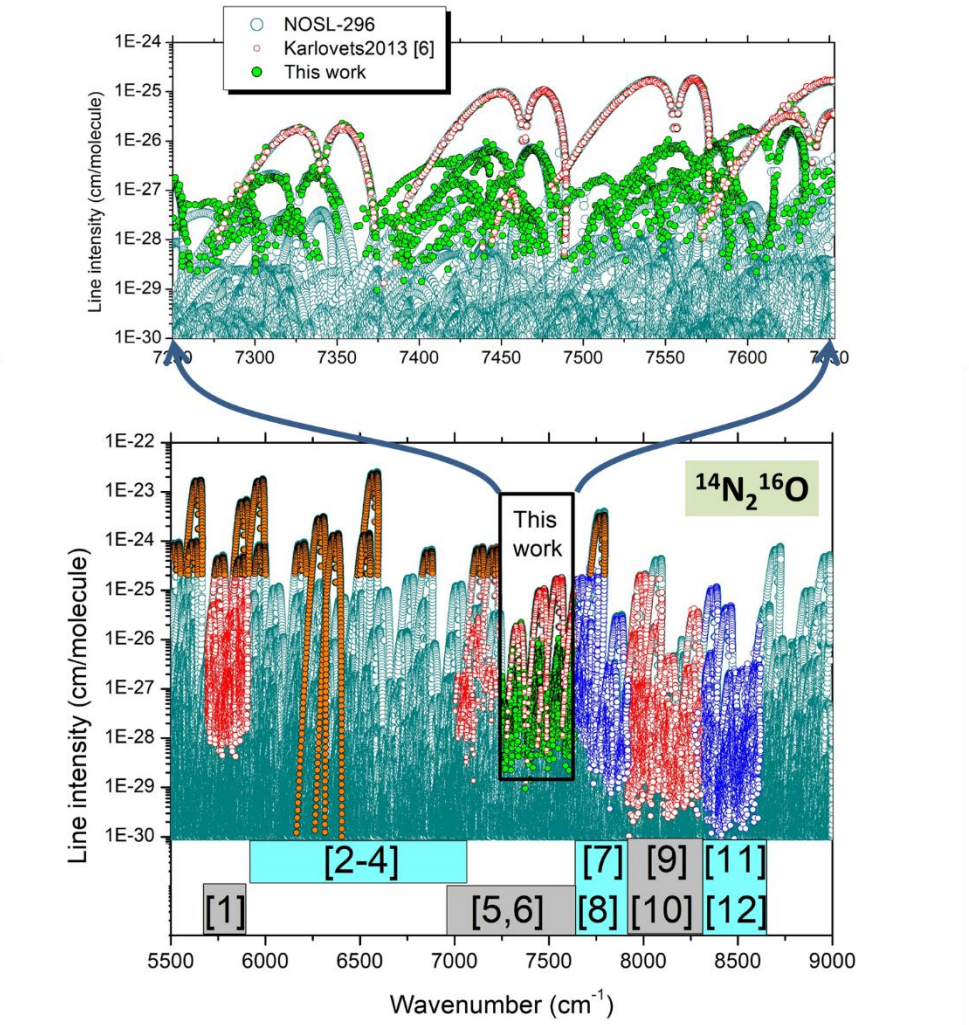

Fig. 1. Overview of various line lists of $^{14}N_2{}^{16}O$ between 5500 and 9000 cm^{-1}.
Lower panel: NOSL-296 [14] and HITRAN2020 [13] line lists (cyan and orange symbols, respectively). The range of previous CRDS investigations is indicated: 5696-5910 cm^{-1} [1], 5905-7066 cm^{-1} [2-4], 6950-7653 cm^{-1} [5,6], 7647-7918 cm^{-1} [7,8], 7915-8334 cm^{-1} [9,10], 8320-8622 cm^{-1} [11,12], and this work. Red and blue circles correspond to CRDS intensities previously reported.
Upper panel: Enlargement corresponding to the 7250 - 7653 cm^{-1} range of the present study. The line intensities of a few bands were previously reported in Ref. [6] (red circles). About 4180 line intensities are retrieved in the present study (light green symbols).

The rest of this paper is organized as follows. The experimental setup and the construction of the measured lists are briefly recalled in Section 2. In Section 3, we present the spectra analysis, the refined band-by-band fitting of the G_v, B_v. D_v, and H_v band parameters and the identification of

resonance perturbations. Finally, in Section 4, the comparison of the experimental data to the NOSL and Ames line lists will allow for discussing their respective advantages and drawbacks.

2. Experimental details

The description of the CRDS recordings has been presented in Refs. [5,6] and is not repeated here. The cavity ring down spectrometer has been described in detail in Refs. [16-18]. The ring down cell (142 cm long) was filled with nitrous oxide in natural isotopic abundance (Air Liquide, Alphagaz, purity ≥ 99.99%). The analyzed spectra were recorded at room temperature (294±0.3 K) with a sample pressure value of 10 Torr. The wavenumber scale of the spectra was calibrated with the help of a lambdameter (Burleigh WA1650) and accurate reference line positions of H_2O (present as an impurity) taken from the HITRAN database [19]. The typical value of the noise equivalent absorption coefficient was $\alpha_{min} \sim 5\times10^{-11}$ cm^{-1} as illustrated on **Fig. 2**

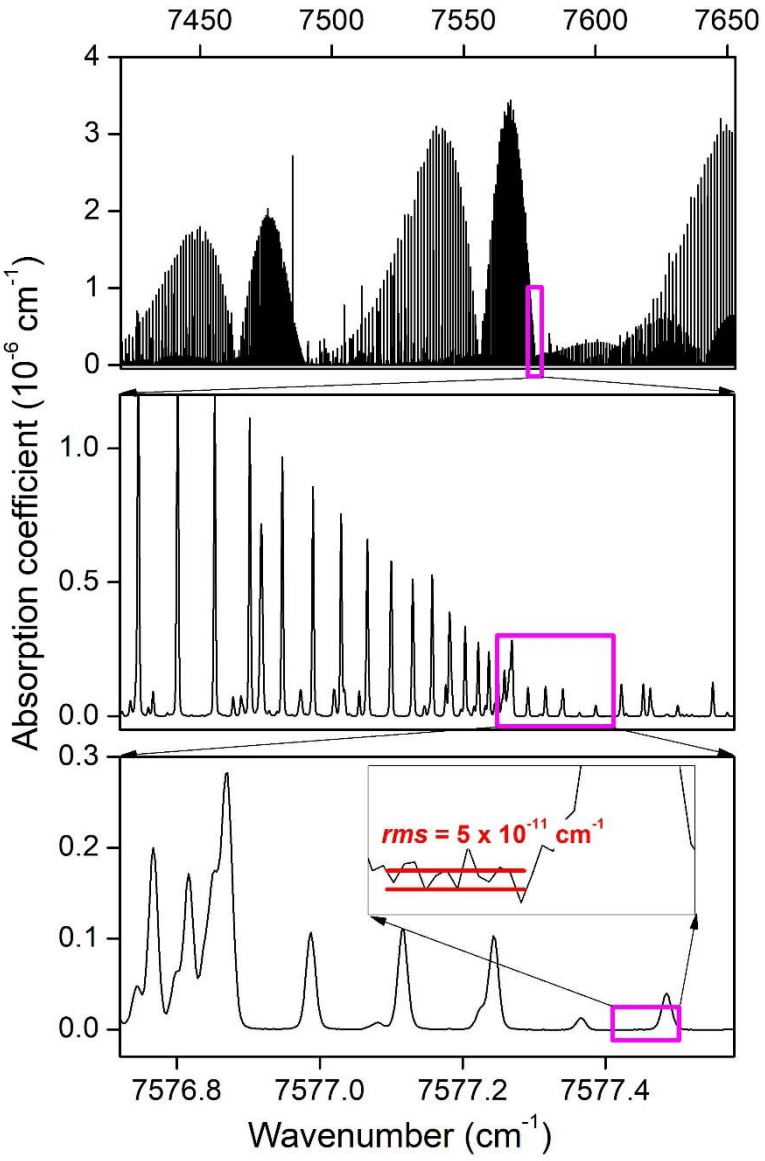

Fig. 2. CRDS spectrum of natural nitrous oxide recorded at a pressure of 10.0 Torr.

The overview of the N_2O spectrum at 10 Torr between 7250 and 7653 cm^{-1} is presented in **Fig. 2**. The noise equivalent absorption on the order of $\alpha_{min} \approx 5\times10^{-11}$ cm^{-1}. It led to the detection of the large number of lines with intensity as small as 10^{-29} cm/molecule involving many hot bands of the main $^{14}N_2{}^{16}O$ isotopologue and the contribution of minor $^{14}N^{15}N^{16}O$, $^{15}N^{14}N^{16}O$, and $^{14}N_2{}^{18}O$ isotopologues in natural isotopic abundance.

A LabVIEW interactive least squares multi-lines fitting program was used to get the line centers and intensities. The line profile was assumed to be of Voigt type with the Gaussian component constrained to the calculated value of the Doppler profile. The fitting process produced the line position, integrated absorbance, Lorentzian widths, and the corresponding local baseline (assumed to be a linear function of the wavenumber).

The complete line list retrieved from the 10 Torr spectra consist of 6656 lines between 7250 and 7653 cm^{-1} with line intensities ranging between 10^{-30} and 2×10^{-25} cm/molecule. Water vapor is present as an impurity in our sample. Due to strong lines located in the region (line intensity up to 1×10^{-20} cm/molecule), 1475 water lines were identified by comparison to the HITRAN spectroscopic database [13], and removed from the list. A set of about 5180 lines was thus left for the rovibrational assignment.

3. Rovibrational analysis

3.1. Rovibrational assignments

A total of 4186 lines belonging to 69 bands of $^{14}N_2{}^{16}O$, $^{14}N^{15}N^{16}O$, $^{15}N^{14}N^{16}O$, and $^{14}N_2{}^{18}O$ were assigned in the 7250-7653 cm^{-1} region. The observed bands correspond to the ΔP= 12-14 series of transitions. In the following, we will label the bands both *(i)* with the traditional $V_1V_2l_2V_3$ normal mode notation where $V_1V_2l_2V_3$ corresponds to the maximum value of the modulo of the expansion coefficients of the eigenfunctions in the normal mode basis and *(ii)* with the cluster labeling notation of the upper state: (P l_2 i) where $P= 2V_1+V_2+4V_3$, l_2 is the quantum number of the angular momentum associated to the vibrational bending mode and i is the order number within the considered polyad increasing with the energy. Due to strong vibrational mixing, the normal mode labeling can be ambiguous while it is not the case for the cluster labeling notation.

As in the previous analysis [5], the assignments were carried out by comparison with the predictions of the effective operator models. In the case of the $^{14}N_2{}^{16}O$ isotopologue, we used the recent NOSL-296 line list [14]. The NOSL list covers the 0.02–13378 cm^{-1} spectral range and contains almost 900,000 lines with line intensities larger than 10^{-30} cm/molecule. This list is based on a non-polyad model of the effective Hamiltonian [20] and effective dipole moment operators [14] with parameters fitted against experimental data. In the studied region, the NOSL line list contains about

16860 $^{14}N_2{}^{16}O$ transitions above an intensity cut-off of 10^{-30} cm/molecule. As the line position values of Ref. [5] were used as input data for the fit of the NOSL EH parameters, the agreement between the NOSL and presently measured position values is expected to be very good (see below).

For minor isotopologues, the $^{14}N^{15}N^{16}O$ and $^{15}N^{14}N^{16}O$ line positions were calculated using the polyad models of the effective Hamiltonian reported in Ref. [21]. The parameters of these models were refitted to the experimental position input files of Ref. [21] supplemented by recently published measurements from Refs. [11,12,22,23]. The same procedure for the EH model of $^{14}N_2{}^{18}O$ published in Ref. [10] was used. The dipole moment parameters of $^{14}N_2{}^{16}O$ [14] were used to fit the measured line intensities of $^{14}N^{15}N^{16}O$ and $^{15}N^{14}N^{16}O$ [9,11,12,15,23-25], and $^{14}N_2{}^{18}O$ [1,10-12,15,25]. Only those parameters that affect the measured intensities were fitted. The remaining parameters were fixed at the corresponding values of the $^{14}N_2{}^{16}O$ EDM parameters. The eigenfunctions of the fitted effective Hamiltonian polyad models were used for the intensity calculations.

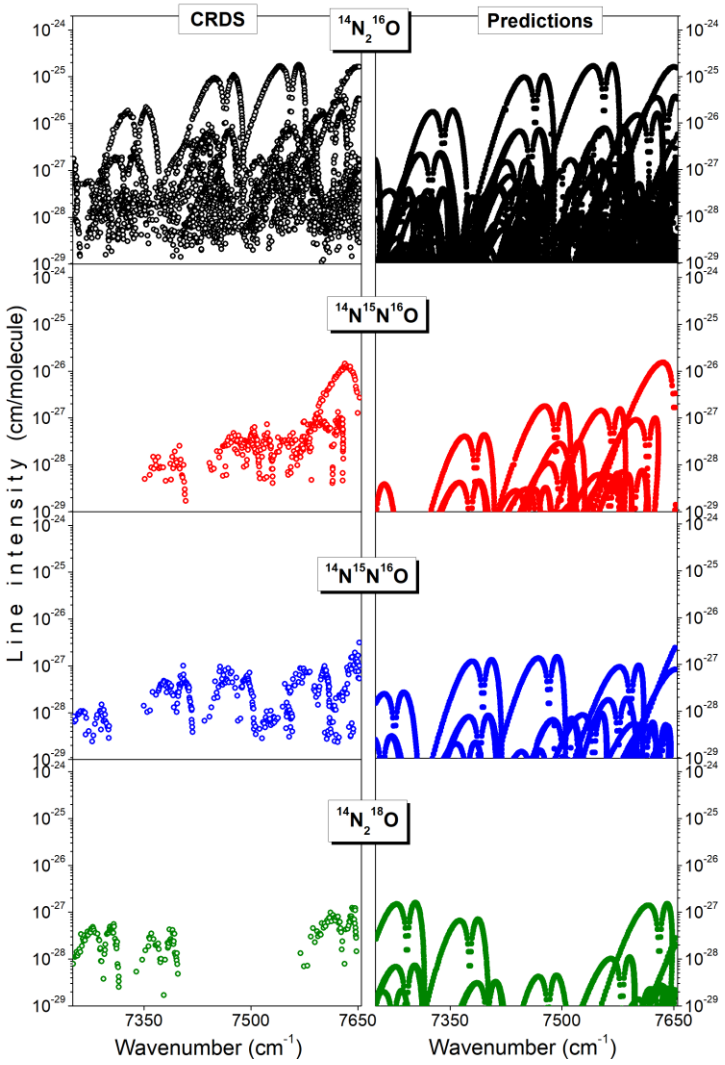

Fig.3. Overview comparison of the measured and predicted line lists of the four nitrous oxide isotopologues contributing to the absorption spectrum between 7250 and 7653 cm^{-1}: $^{14}N_2{}^{16}O$ (446),

$^{14}N^{15}N^{16}O$ (456), $^{15}N^{14}N^{16}O$ (546), and $^{14}N_2{}^{18}O$ (448). Note that the line intensities are plotted in logarithmic scale and include the isotopic abundance factor.

Fig. 3 shows the overview comparison of the CRDS observations of the four N_2O isotopologues contributing to the analyzed spectrum, to the predictions of their respective effective operator models. About 990 very weak lines (intensity less than 10^{-29} cm/molecule) were left unassigned at the final stage of the assignment process.

Table 1 summarizes the number of transitions and bands measured in this work. Overall, seven $^{14}N_2{}^{16}O$ bands and one $^{15}N^{14}N^{16}O$ band are newly reported. Their vibrational assignment is marked with bold character in **Table 2**. Both the normal mode and (*P l*$_2$ *i*) cluster labeling assignments are given for each band in **Table 2**. Note that we correct here a ten of erroneous values of the *i* ranking number given in Ref. [5],

Table 1. Number of transitions and bands of the different N_2O isotopologues measured in the 7250–7653 cm^{-1} region.

Molecule	HITRAN notation	Abundance [13]	Number of transitions	Number of bands [a]
$^{14}N_2{}^{16}O$	446	9.903×10^{-1}	3328	51(7)
$^{14}N^{15}N^{16}O$	456	3.641×10^{-3}	359	6(0)
$^{15}N^{14}N^{16}O$	546	3.641×10^{-3}	325	8(1)
$^{14}N_2{}^{18}O$	448	1.986×10^{-3}	174	4(0)
Total			**4186**	**69(8)**

Note:

[a] The number within parentheses correspond to newly assigned bands.

The N_2O assigned line list provided as Supplementary Material, includes the isotopologue identification, rovibrational assignment, measured line parameters, and corresponding values predicted by the effective operator models. For comparison purpose, the Ames line parameters are also included (see **Section 4)**.

3.2. Band-by-band analysis

As usual, we used the following equation of the vibration-rotational energy levels to fit the upper state spectroscopic parameters to the observed wavenumbers:

$$F_v(J) = G_v + B_vJ(J+1) - D_vJ^2(J+1)^2 + H_vJ^3(J+1)^3 \quad (1)$$

where G_v is the vibrational term value, B_v is the rotational constant, D_v and H_v are the centrifugal distortion constants, J is the angular momentum quantum number. In the case of hot bands, the *e* and *f* sub-bands were considered independently. The results of the band-by-band fit of the spectroscopic parameters are given as a Supplementary Material. The lower state constants were constrained to their literature values from Refs. [15,26] and are included in the Supplementary

Material. A total of 68 bands were fitted. The typical *rms* value of the fits is about 6×10^{-4} cm^{-1}, which is consistent with our claimed accuracy on the line positions (~ 10^{-3} cm^{-1}).

The retrieved constants ordered according to the band centers are listed in **Table 2**, for the four isotopologues. In the case of bands located near the borders of the investigated region, the input data set was supplemented with measurements from Refs. [5,8]. All these lines are indicated with their source in the Supplementary Material.

3.3. Local rovibrational perturbations

Eight $^{14}N_2{}^{16}O$ bands were found affected by local Coriolis or anharmonic interactions. Five of these interactions are evidenced for the first time. For some previously analyzed perturbations, we could newly assign some extra lines. The corresponding perturbed transitions were excluded from the fit of the spectroscopic constants. The perturbations were identified on the basis of the NOSL-296 line list [14]. **Table 3** lists for each of the perturbed bands, their center, the coupling mechanism, the *J* values corresponding to the energy crossing of the interacting states (J_{cross}), and the number of extra lines assigned in this work. When available, the references where these perturbations were firstly reported is given in the last column of **Table 3**.

Table 3. Observed local rovibrational perturbations of $^{14}N_2{}^{16}O$ bands between 7250 and 7653 cm^{-1}.

Affected band	Center (cm^{-1})	Interacting states[a]	Interaction mechanism	J_{cross}	Number of extra lines	*Ref.*[b]
2112e-0000e 2112f-0000e	7443.008	(13 1 7) ↔ (13 1 6)	Intrapolyad anharmonic	17	6 3	[4,5]
6000e-0000e	7463.985	(12 0 14) ↔ (12 3 5)	Intrapolyad Coriolis	36	2	TW
6200e-1000e	7525.861	(14 0 19) ↔ (16 0 3)	Interpolyad anharmonic	24	11	[5]
6110e-0110e 6110f-0110f	7570.895	(13 1 15) ↔ (14 2 9) (13 1 15) ↔ (14 2 9) (13 1 15) ↔ (14 2 6) (13 1 15) ↔ (14 0 11)	Interpolyad Coriolis Interpolyad Coriolis Interpolyad Coriolis Interpolyad Coriolis	*e*: 17 *f*: 21 *e*: 27 *e*: 37	6 6 19 0	[5] [5] [5] TW
2113e-1110e 2113f-1110f	7657.001	(17 1 7) ↔ (15 1 11)	Interpolyad anharmonic	31	0	TW
1004e-0001e	7664.811	(18 0 4) ↔ (18 0 3) (18 0 4) ↔ (17 1 10)	Intrapolyad anharmonic Interpolyad Coriolis	13 35	0 0	TW TW
2003e-1000e	7691.585	(16 0 7) ↔ (16 0 6)	Intrapolyad anharmonic	32	1	[4,5,8]
1223e-0220e 1223f-0220f	7710.775	(16 2 3) ↔ (15 1 13)	Interpolyad Coriolis	*e*:32 *f*: 32	0 0	[4,5,8]

Notes

[a] Cluster labeling notation.

[b] First report of the considered perturbation. (TW: This work).

Fig. 4 shows the effect of the anharmonic resonance interaction between the (13 1 7) and (13 1 6) states on the rotational structure of the R branch of the 2112e-0000e band [the cluster labeling

notation of the upper state of this band is (13 1 7)]. The differences between the measured line positions of the 2112e-0000e band and those provided by NOSL-296 [14] or calculated using the spectroscopic parameters (SP) of **Table 2** are plotted on the lower panels. A total of six extra lines (R12, R14, R15, R16, R18, R21) belonging to the 0911e upper state [(13 1 6) in cluster labeling notation] could be identified around the energy crossing J_{cross} = 17. We also assigned three extra lines (Q16, Q17, and Q18) in the *Q* branch of the 2112f-0000e sub-band. The extra lines are provided in the Supplementary Materials. The comparison of the two lowest panels (plotted with different Y-axis scales) illustrates the quality of the NOSL-296 line positions in the present case of an intrapolyad interaction. The measured line positions (including extra lines) are reproduced within typically 10^{-3} cm^{-1} while the position perturbation of the R15 and R16 transitions of the bright 2112e-0000e band exceeds 0.1 cm^{-1}.

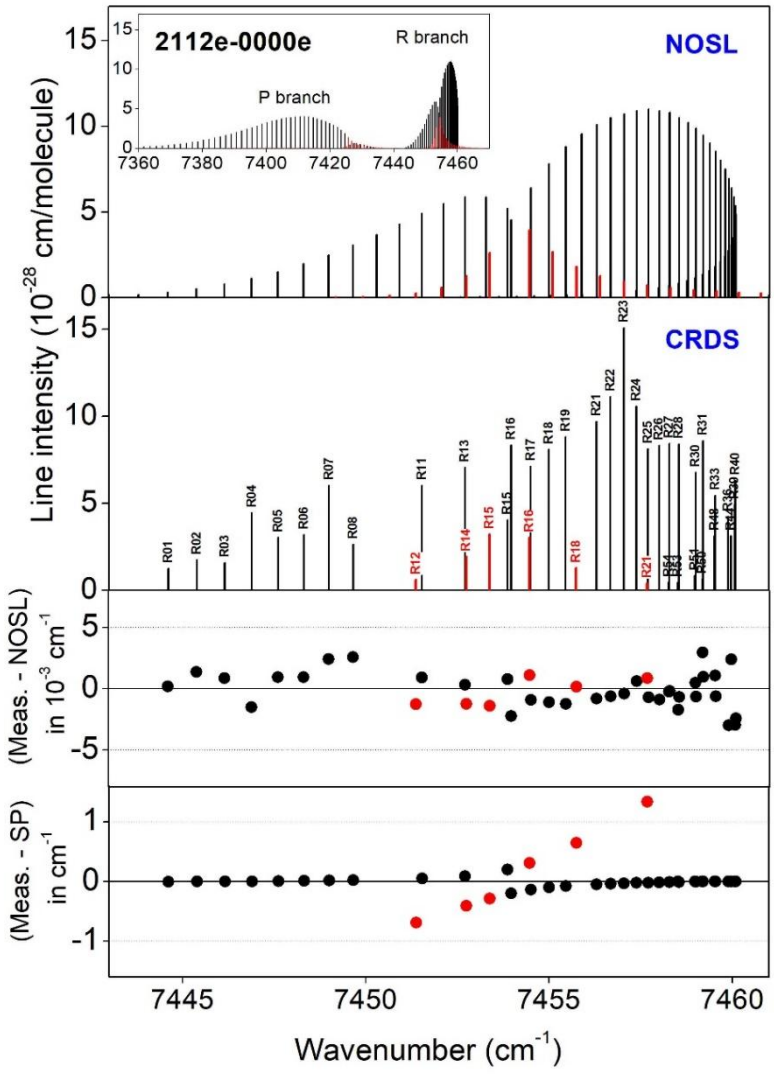

Fig. 4. The perturbed *R(J)* branch of 2112e-0000e band of $^{14}N_2{}^{16}O$ at 7443.008 cm^{-1}.
Upper panels: Overview of the NOSL-296 and experimental stick spectra of the *R(J)* branch of 2112e-0000e band. The (13 1 7) upper state is perturbed by an anharmonic interaction with the (13 1 6)

state (energy crossing at J_{cross} = 17). The extra lines (R12, R14, R15, R16, R18, R21) belong to the 0911e-0000e band and are marked in red.
Lower panels: Differences between the CRDS line positions and those provided by NOSL-296 [14] and the values calculated using the spectroscopic constants (SP) of **Table 2**.
Note the different Y-axis scales of the two lower panels.

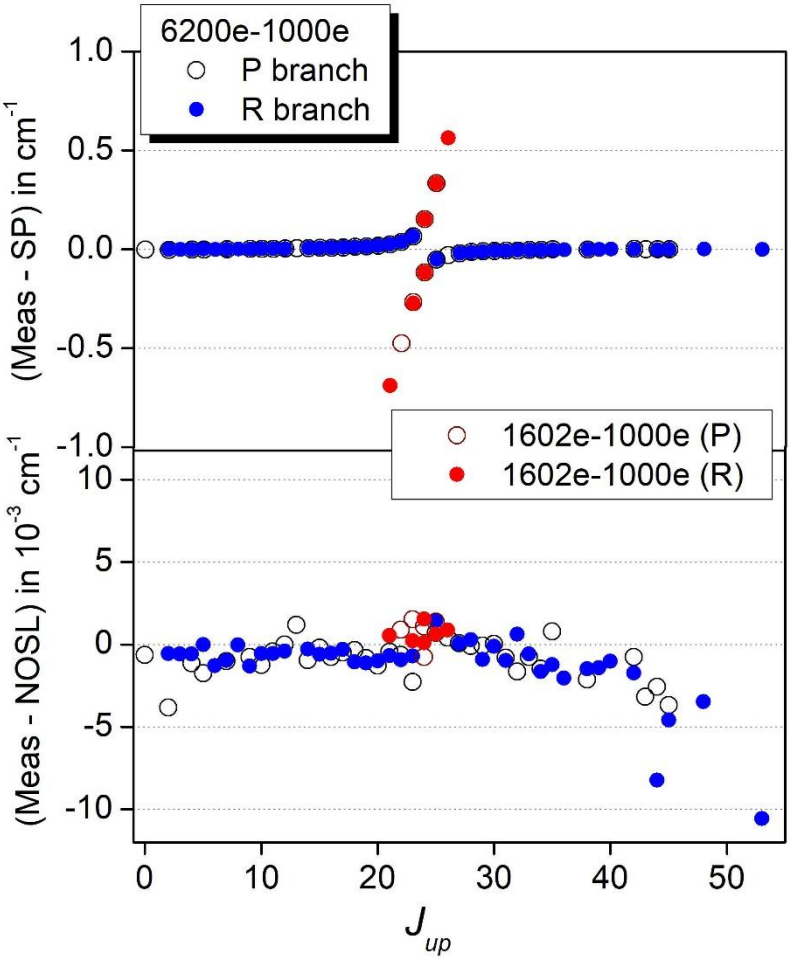

Fig. 5. Perturbation of the line positions of the 6200e-1000e band of $^{14}N_2{}^{16}O$ centered at 7525.861 cm^{-1}. The residuals between the measured line positions and the values calculated using the spectroscopic constants of **Table 2** and provided by NOSL-296 [14] are plotted *versus* the *J* rotational quantum number of the upper energy level. An interpolyad anharmonic resonance interaction between the (14 0 19) and (16 0 3) vibrational states is responsible of the observed position perturbations around the *J* crossing value of 24. A total of 11 extra lines belonging to the 1602e-1000e band could be detected (*P branch*: brown empty circles, *R branch:* red full circles).

The 6200e-1000e band at 7525.861 cm^{-1} reaching the (14 0 19) upper state is perturbed by an anharmonic resonance interaction with the (16 0 3) perturber state (energy crossing at J_{cross}= 24). This interpolyad perturbation was firstly analyzed in Ref. [5]. Here, we could newly identify eleven extra lines (*P*23-*P*26 and *R*22-*R*25) due to an intensity transfer towards the 1602e-1000e band. The residuals between the measured line positions of the 6200e-1000e band and those calculated by using the spectroscopic constants of **Table 2** and provided by NOSL-296 [14] are presented in **Fig. 5.**

On this figure, the deviations are plotted *versus* the rotational quantum number of the upper state of the transition, J_{up}. As a given upper state J_{up} level can be accessed through both P- and R-transitions, coincident deviation values for $P(J_{up}+1)$ and $R(J_{up}-1)$ insure that lower state combination difference relations are fulfilled. This agreement was particularly valuable to validate the assignment of the extra lines. As in the previous example, the NOSL predictions agree with the observations within about the experimental uncertainty on the line position (about 1×10^{-3} cm^{-1}). Nevertheless, here the interaction mechanism involves states belonging to different polyads (P= 14 and 16) and only recently a non-polyad model of the effective Hamiltonian has been developed for $^{14}N_2{}^{16}O$ to account for interpolyad interactions [20]. This model is the one used to generate the NOSL-296 position values.

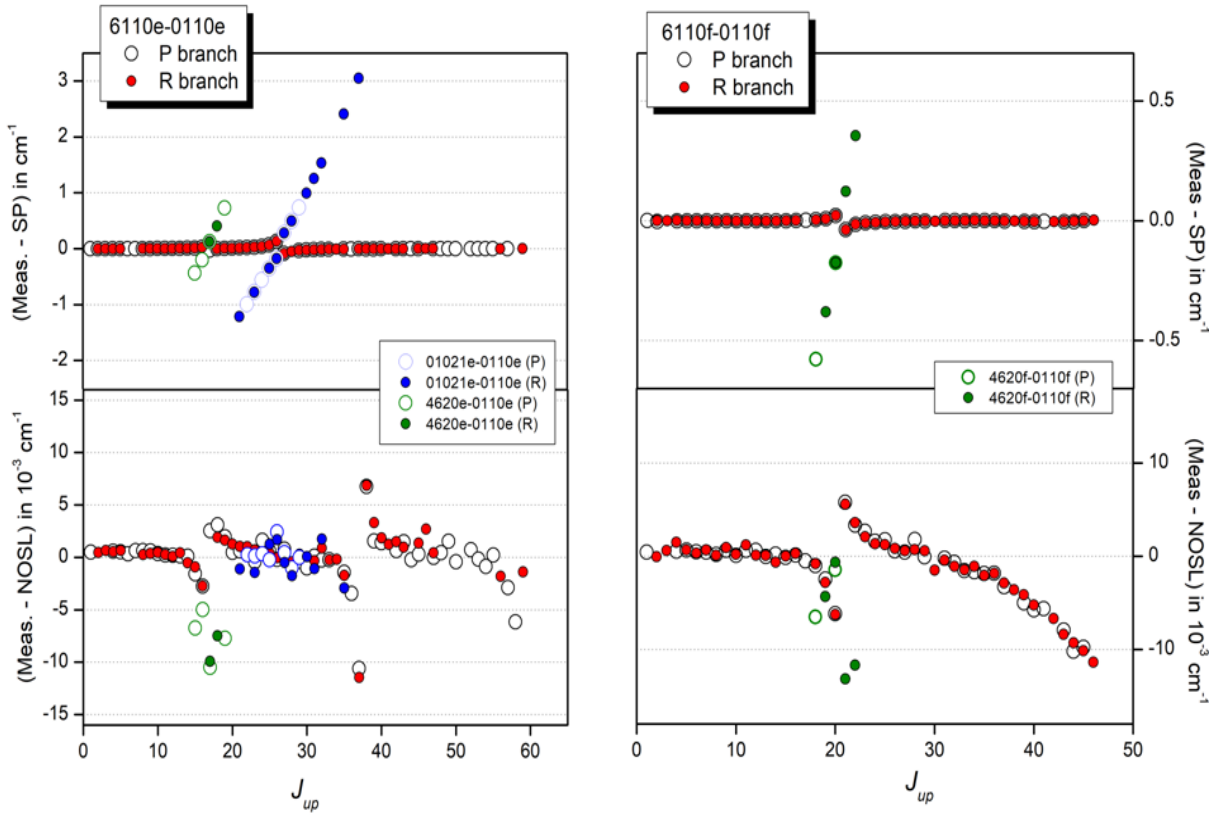

Fig. 6. Differences between the measured line positions of the 6110-0110 hot band at 7570.895 cm^{-1} and the corresponding values calculated using the spectroscopic constants (SP) of **Table 2** (upper panels) and provided by NOSL-296 [14] (lower panels) for the *e* and *f* sublevels, respectively.
Left hand: The (13 1 15) upper state is perturbed by interpolyad Coriolis interactions with *(i)* (14 2 9) around J_{cross} = 17; *(ii)* (14 2 6) around J_{cross} = 27, and *(iii)* (14 0 11) around J_{cross} = 37.
Right hand: The (13 1 15) upper state is perturbed by interpolyad Coriolis interaction with (14 2 9) around J_{cross} = 21.

The (13 1 15) state is the upper state of the 6110-0110 hot band at 7570.895 cm^{-1} which shows several local perturbations, all due to interpolyad Coriolis interactions with: (*i*) the (14 2 9) state (J_{cross} = 17 and 21 for *e* and *f* sublevels, respectively), (*ii*) the (14 2 6) state (J_{cross} = 27), and (*iii*) (14 0 11) state (J_{cross} = 37). Most of these perturbations were first evidenced in Ref. [5]. Here, we could newly

evidence the interpolyad Coriolis resonance around the energy crossing at J = 37 and a total of 31 extra lines were identified: twelve extra lines belonging to the 4620-0110 band [(14 2 9) upper state in cluster labeling notation] could be assigned around the J crossing values 17 and 21 for *e* and *f* sublevels, respectively and 19 extra lines were assigned around J_{cross} = 27. These lines are due to an intensity transfer towards the 0(10)21-0110 band [(14 2 6) upper state in cluster labeling notation]. The residuals between the measured line positions of the 6110-0110 band and those calculated by using the spectroscopic constants of **Table 2** and provided by NOSL-296 [14] are presented in **Fig. 6** (*e-e* and *f-f* sub bands are presented on the left and right panels, respectively). The NOSL predictions allow accounting satisfactorily of the different perturbations. Nevertheless, some significant residuals remain near J_{cross}= 17 and 37 and J_{cross} = 21 for the *e-e* and *f-f* sub bands, respectively. It may indicate that the EH parameters of the non-polyad model should be slightly refined to reproduce the line positions within the experimental uncertainty.

4. Comparison with the NOSL-296 and Ames calculated line lists

4.1. $^{14}N_2{}^{16}O$

We present in **Fig. 7** an overview comparison for the measured $^{14}N_2{}^{16}O$ line positions. From top to bottom, the experimental data are compared to *(i)* the NOSL-296 values [14], *(ii)* the values calculated using the spectroscopic constants of **Table 2**, and *(iii)* the Ames-296 values [**27**]. **Fig.7** presents two columns: in the right panels, all the position measurements are considered for the different comparisons while in the left panels, the comparisons are limited to the lines whose positions were included in the fit of the band-by-band spectroscopic parameters listed in **Table 2** (let us call these lines “SP lines”, hereafter). Thus, the positions of perturbed or poorly determined lines are excluded from the left panels. SP lines have their positions well reproduced by the band-by-band fits of the SP parameters (|meas. – calc.| position difference smaller than 10^{-3} cm^{-1}) and the excluded lines are clearly evidenced by the comparison of the middle panels.

Let us recall that the NOSL and Ames calculated lists were obtained with very different theoretical approaches. While the NOSL list is based on effective operators with parameters fitted against measured line positions and line intensities, the Ames list is based on an empirical potential energy surface (PES) and a pure *ab initio* dipole moment surface. In the following comparison, we will use the Ames-296 line list available at http://huang.seti.org with file name n2o.6iso.296K.1E-31.15Kcm-1.Y02-A8.dmsC.dat.

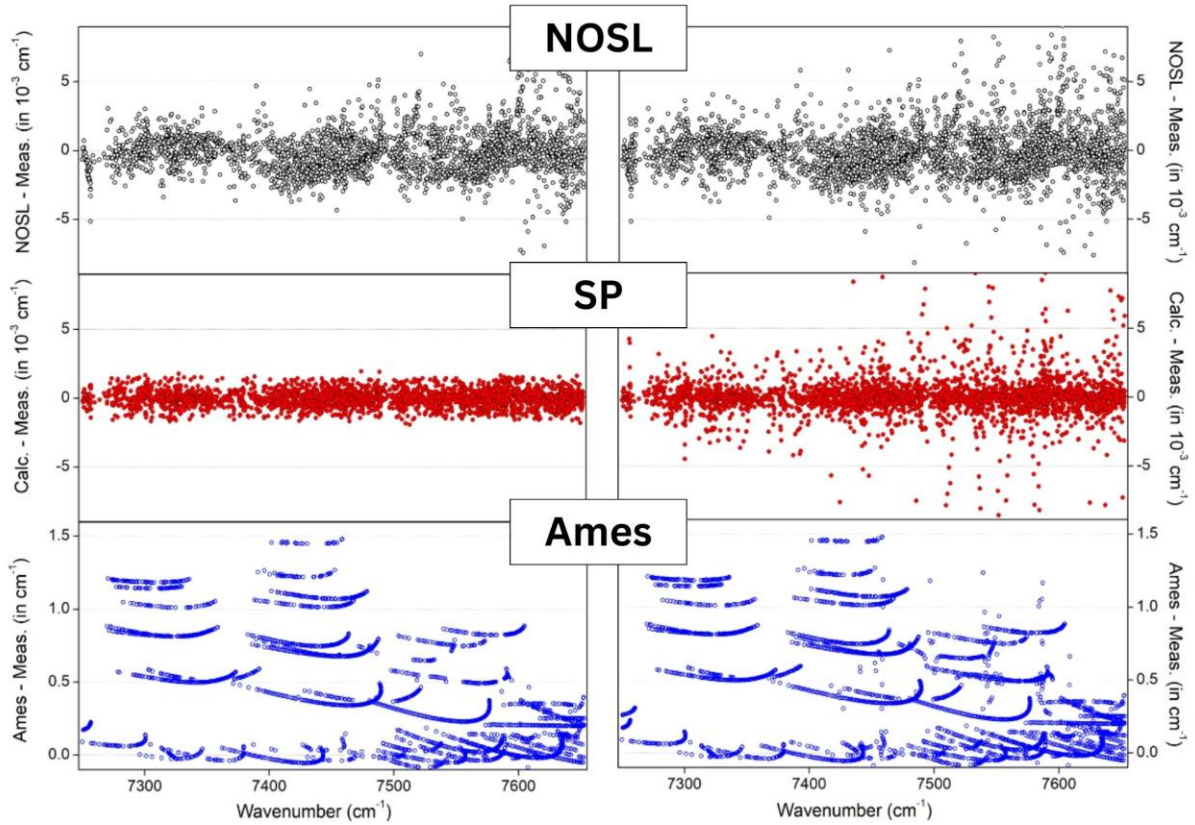

Fig. 7. Position differences between the measured and the calculated line lists between 7250 and 7653 cm^{-1}: (*i*) NOSL-296 [14] (upper panels), (*ii*) calculated using the band-by-band spectroscopic constants of Table 2 (SP) (middle panels), (*iii*) Ames-296 [27] (lower panels).
Right hand: all the experimental lines are shown. *Left hand*: only the lines that are included in the fit of the spectroscopic constants are shown.
Note the different Y-axis scales of the panels.

As expected, the comparison of the lower and upper panels of **Fig. 7** illustrates the fact that the accuracy of the Ames positions cannot compete with the NOSL (and SP) position accuracy. The Ames deviations are mostly band dependent with a limited rotational dependence. On average, Ames term values of the upper vibrational states involved in the considered bands appear to be overestimated, by an amount up to 1.5 cm^{-1}. Although limited, the rotational dependence of the deviations is clear and systematic. The Ames rotational energies are overestimated by amounts increasing with J up to about 0.2 cm^{-1}.

As most of the presently measured line positions were previously reported in Ref. [5] and thus included in the transition dataset used to fit the EH parameters [20], the NOSL line positions are in close agreement to the observations even in case of interpolyad interaction (see above). Nevertheless, as concerns SP lines (for which SP calculated positions deviate by less than 10^{-3} cm^{-1}), the comparison of the two upper left panels of **Fig. 7** seems to indicate that the band-by-band SP

parameters allow for a slightly better reproduction of the measured positions than the (non-polyad) EH model, the NOSL position deviations of some SP lines near 7600 cm^{-1} being on the order of 5×10^{-3} cm^{-1}.

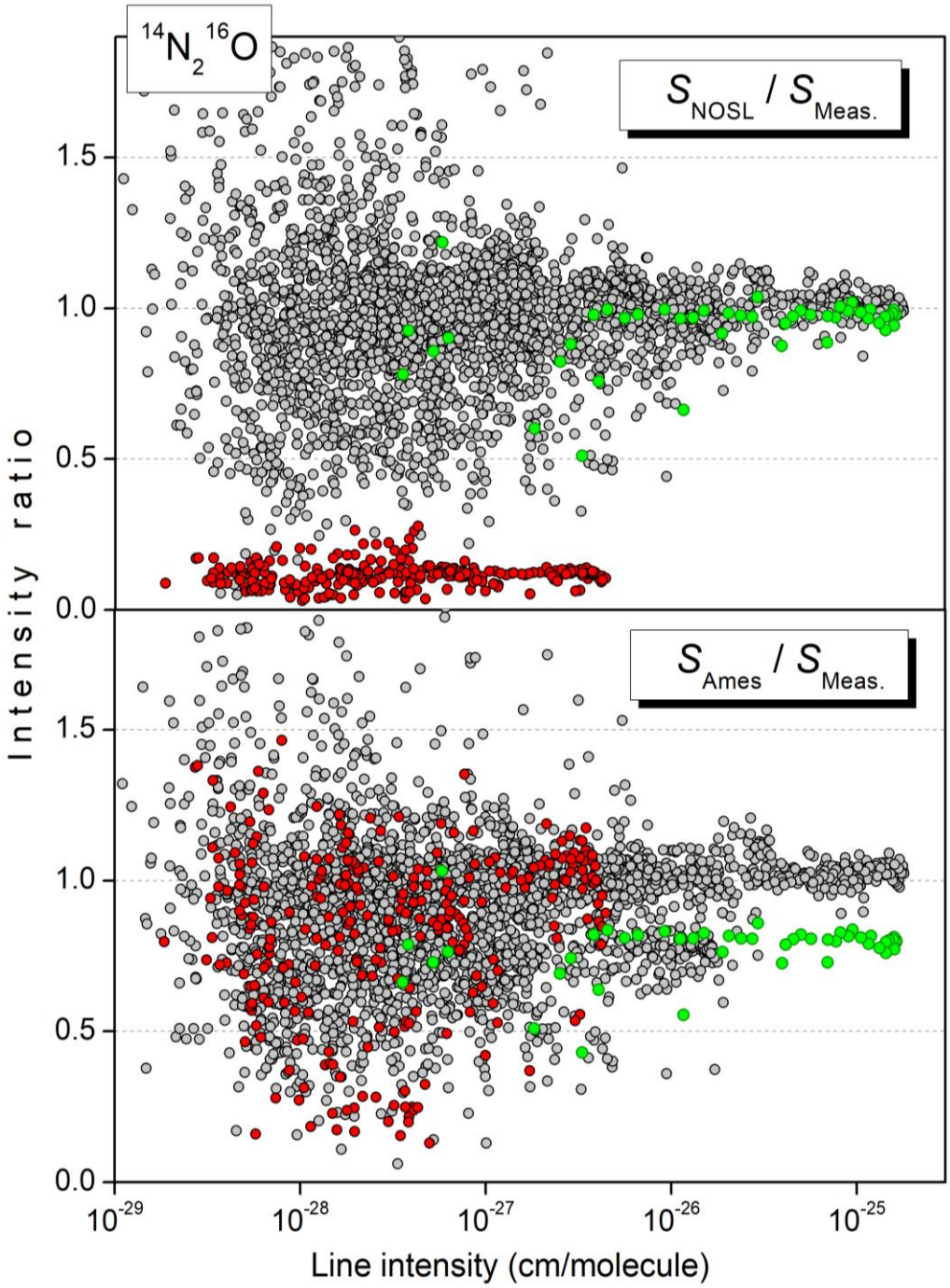

Fig. 8. Variation of the ratio of the calculated and measured line intensities *versus* the measured intensity values of the $^{14}N_2\,^{16}O$ transitions in the 7250-7653 cm^{-1} region. The 0203-0000 band is plotted with green full circles. Six ΔP = 14 bands (0004-0200, 0004-1000, 0403-1000, 2112-0000 (*Q* branch), 0114-0310, and 0114-1110) with strongly underestimated NOSL intensities are plotted with red full

circles. Upper and lower panels are relative to the NOSL-296 [14] and Ames [27] databases, respectively.

The comparison of the measured $^{14}N_2{}^{16}O$line intensities to those provided by NOSL-296 [14] and Ames-296 [27] line lists is presented in **Fig. 8**. The overall agreement is good for both calculated lists but each of them shows important deviations for some specific bands. The most obvious problem concerns the NOSL intensity of a series of ΔP = 14 bands, namely 0004-0200, 0004-1000, 0403-1000, 2112-0000 (*Q* branch), 0114-0310, and 0114-1110 – which have their NOSL line intensities underestimated by about one order of magnitude (red symbols in **Fig. 8**). The intensity of these bands is mainly determined by the $M^0_{-1,0,4}$ EDM parameter which, due to the lack of intensity information, could not be determined in the global fit of the EDM parameters used to generate NOSL intensities. The present intensity measurements will allow correcting this issue. We note that, in spite of a high dispersion of the intensity ratios, the Ames intensities do not show a similar problem for the considered ΔP = 14 bands (red dots in the lower panel of **Fig. 8**).

At the opposite, the NOSL line intensities of the 0203e-0000e band centered at 7665.273 cm^{-1} agree with the measurements while the Ames intensities are systematically underestimated by about 20 % (green dots in **Fig. 8**). According to Dr. X. Huang from the Ames team, this band is "a sensitive band which intensity may vary by 15-50% according to the dipole moment surface". Note that the agreement observed between the NOSL intensities and the measurements is not surprising because this band is one of the bands for which intensity information was reported in Ref. [6] and used to derive the EDM ΔP = 14 parameters of the NOSL database.

4.2. $^{14}N^{15}N^{16}$, $^{15}N^{14}N^{16}O$, and $^{14}N_2{}^{18}O$

Fig. 9 shows the overview comparison of the CRDS line positions for the $^{14}N^{15}N^{16}O$, $^{15}N^{14}N^{16}O$, and $^{14}N_2{}^{18}O$ isotopologues to the effective Hamiltonian positions and the Ames-the NOSL list is limited to the main isotopologue and the origin of the EH parameters used for each of the considered minor isotopologue has been detailed in section 3.1. The largest ($\nu_{EH} - \nu_{CRDS}$) deviations are about 5×10^{-3} cm^{-1} for the three minor isotopologues whereas the Ames line positions show deviations with similar general appearance as for $^{14}N_2{}^{16}O$ and an amplitude up to 0.7 cm^{-1}.

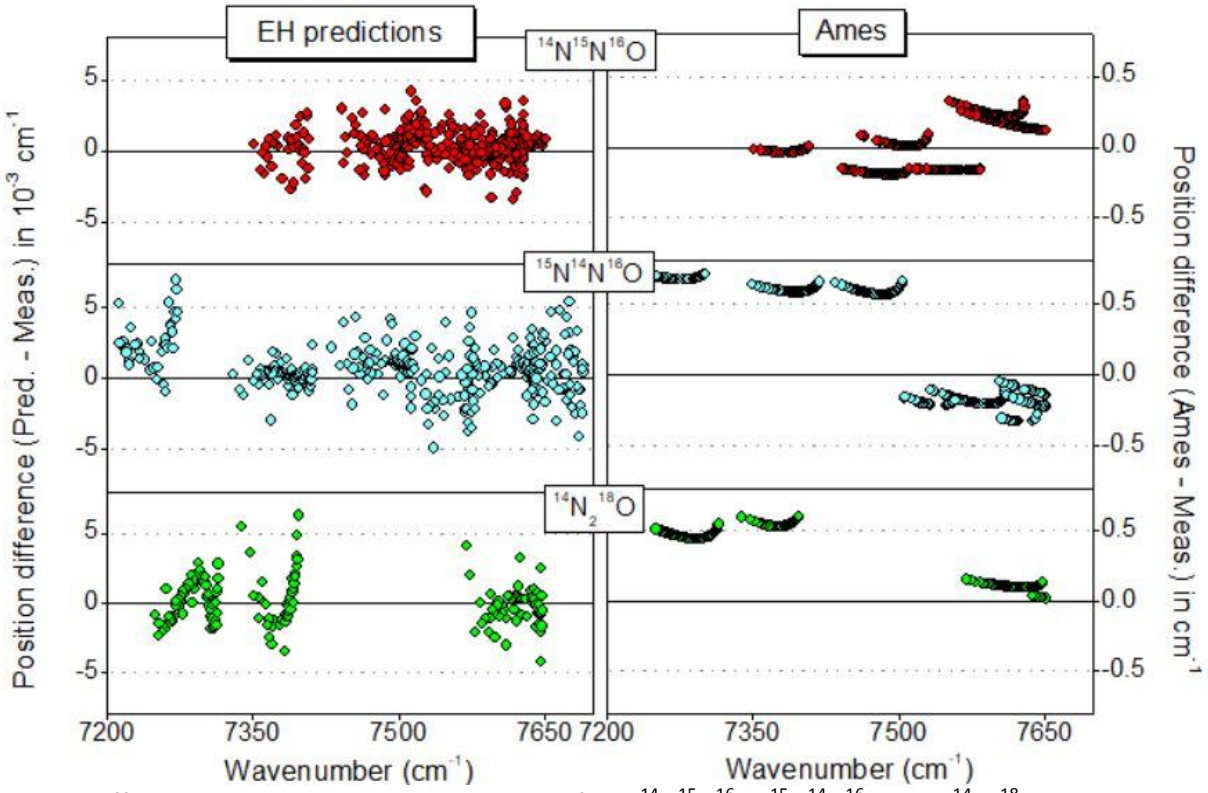

Fig. 9. Differences between the line positions of the $^{14}N^{15}N^{16}O$, $^{15}N^{14}N^{16}O$, and $^{14}N_2{}^{18}O$ isotopologues assigned between 7250 and 7653 cm^{-1} and their values predicted by the effective Hamiltonian (left panels) and Ames database (right panels). Note the different Y-axis scales of the left-hand and right-hand panels.

The ratios of the line intensities predicted by the effective operator model and provided in the Ames list to those measured in this work are presented in **Fig. 10**. Note that due to the low relative abundance values (see **Table 1**), the bands observed for these minor species are all weak (intensity smaller than 2×10^{-26} cm/molecule). They belong to the ΔP = 12 and ΔP = 14 series. Overall, considering the weakness of the considered lines, the agreement with the Ames intensity values is satisfactory for the three minor isotopologues. As concerns line intensities calculated using the effective operator approach, a satisfactory agreement is also observed for the intensities of the ΔP = 14 bands but the line intensities of the 5200e-0000e and 6000e-0000e bands (ΔP = 12) are largely overestimated (by a factor of 2 to 4). The line intensities of these bands were calculated using the corresponding dipole moment parameters of the main isotopologue, $^{14}N_2{}^{16}O$ [14]. As a result, the quality of predictions for these ΔP = 12 bands is low. Although the Ames/meas. intensity ratios show significant dispersion (mostly due to experimental uncertainty related to the weakness of the considered lines), the overall agreement is satisfactory. This observation is of importance to insure that the isotopic abundance in the used N_2O sample is close to its natural value. Indeed, while the chemical purity of the sample is characterized, no information on the isotopic abundance is generally provided by

the gas supplier. The Ames intensity values allow validating the normal isotopic abundance which is generally assumed by default.

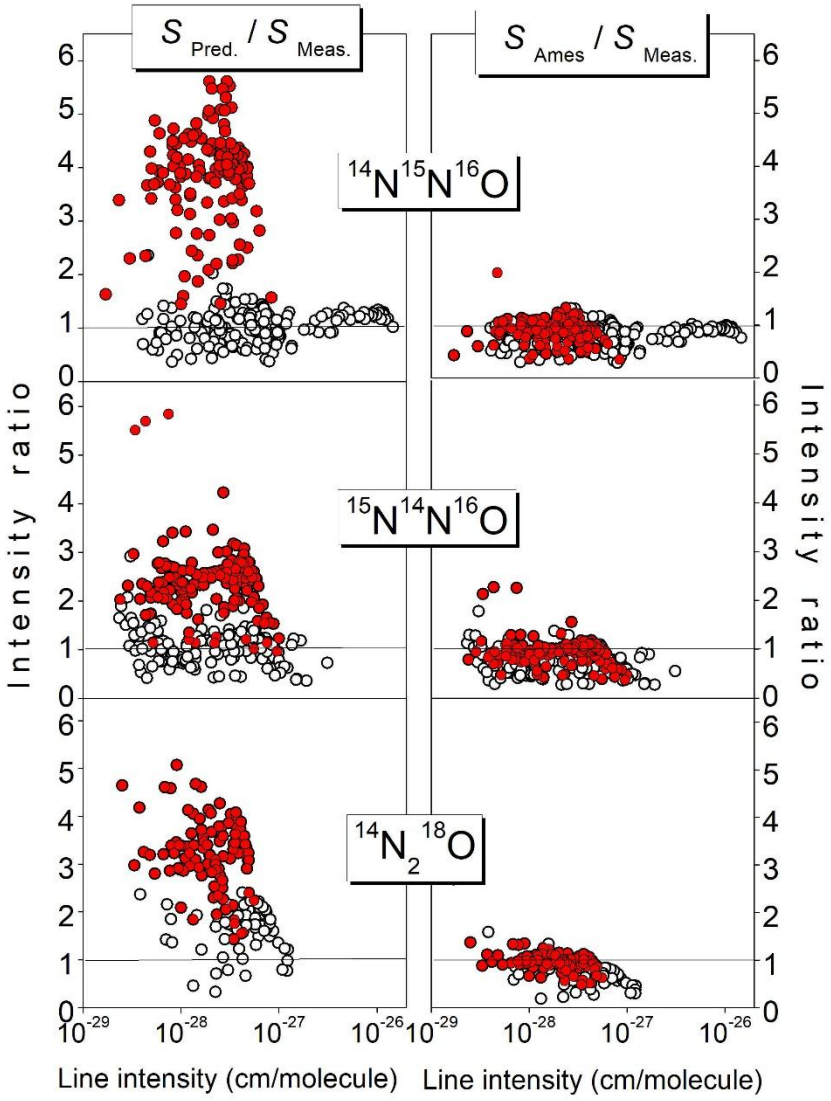

Fig. 10. Ratios of the line intensities predicted by the effective operator model (left panels) and provided by the Ames database (right panels) to the values measured for the $^{14}N^{15}N^{16}O$, $^{15}N^{14}N^{16}O$, and $^{14}N_2{}^{18}O$ isotopologues in the 7250 - 7653 cm^{-1} spectral region. All the bands belong to the ΔP = 14 series except for the 5200e-0000e and 6000e-0000e bands which belong to ΔP = 12 series (red full circles).

5. Conclusion

The absorption spectrum of nitrous oxide has been reconsidered in the 7250 - 7653 cm^{-1} interval. The systematic retrieval of the line parameters using a multiline fit combined with improved predictions of the N_2O absorption spectrum have allowed to identify eight additional bands not reported in Ref. [5], to identify or extend the analysis of rovibrational interaction affecting a few bands and to tests the NOSL-296 list of $^{14}N_2{}^{16}O$ and the Ames line list for all the isotopologues, in particular for line intensities.

The HITRAN database does not provide any line parameters in the region. The comparison validates the quality of the NOSL list of $^{14}N_2{}^{16}O$ in the region. This can be partly explained by the fact that line positions [5] and part of the line intensities [6] were already considered in the transition database used to refine the effective operator model used to generate NOSL. The large set of 3328 intensities presently reported are overall in good agreement with NOSL intensities while only 741 lines were measured in Ref. [6], illustrating the good extrapolation capabilities of the effective operator approach. Nevertheless, six weak ΔP = 14 bands have their NOSL line intensities underestimated by about one order of magnitude compared to measurements because their intensities were not previously measured and relevant ΔP = 14 EDM parameters could not be determined. For the considered bands the Ames intensities are validated by the measurements. Unfortunately, while Ames intensity calculations are found in general very good, the Ames intensities of the 0203-0000 band, which is one of the strongest of the region, are underestimated by about 20 %. Ideally, the best database for N_2O could be obtained by combining the advantages of the NOSL and Ames intensities. For line positions, no doubt that the NOSL values should be preferred. As concerns line intensities, the choice of the best source is less obvious and would require to systematically identify the NOSL bands with unreliable intensities due to the lack of intensity formation and the Ames "sensitive" bands for which intensity calculations may be less accurate. Let us not that the quality of the NOSL intensities benefits from the large experimental information in the near infrared investigated by CRDS (see **Fig. 1**). The advantages of the Ames intensities against NOSL are expected to be more obvious at higher energy where much less experimental data are available.

The above considerations relative to the main isotopologue, apply also to the minor species. In case of experimental data too sparse to determine the EDM parameters of a ΔP series of transitions, the Ames intensity values appear to be preferable.

Acknowledgements

This project is supported by CNRS (France) in the frame of the International Research Project "SAMIA". Sergey Tashkun acknowledges The Ministry of Science and Higher Education of the Russian Federation for financial support. Most of the computations presented in this paper were performed using the GRICAD infrastructure (https://gricad.univ-grenoble-alpes.fr), which is supported by Grenoble research communities.

References

1. Bertin T, Mondelain D, Karlovets EV, Kassi S, Perevalov VI, Campargue A. High sensitivity cavity ring down spectroscopy of N_2O near 1.74 μm. J Quant Spectrosc Radiat Transf 2019;229:40–9. doi:10.1016/j.jqsrt.2019.02.011.
2. Liu AW, Kassi S, Perevalov VI, Tashkun SA, Campargue A. High sensitivity CW-cavity ring down spectroscopy of N_2O near 1.5 μm (II). J Mol Spectrosc 2007;244:48-62. doi:10.1016/j.jms.2007.05.010.
3. Liu AW, Kassi S, Malara P, Romanini D, Perevalov VI, Tashkun SA, Hu SM, Campargue A. High sensitivity CW-cavity ring down spectroscopy of N_2O near 1.5 μm (I). J Mol Spectrosc 2007;244:33-47. doi:10.1016/j.jms.2006.03.007.
4. Liu AW, Kassi S, Perevalov VI, Hu SM, Campargue A. High sensitivity CW-cavity ring down spectroscopy of N_2O near 1.5 μm (III). J Mol Spectrosc 2009;254:20–7. doi:10.1016/j.jqsrt.2019.02.011.
5. Lu Y, Mondelain D, Liu AW, Perevalov VI, Kassi S, Campargue A. High Sensitivity CW-Cavity Ring Down Spectroscopy of N_2O between 6950 and 7653 cm^{-1} (1.44-1.31 μm): I. Line positions. J Quant Spectrosc Radiat Transfer 2012;113:749-62. doi:10.1016/j.jqsrt.2012.03.005.
6. Karlovets EV, Lu Y, Mondelain D, Kassi S, Campargue, Tashkun SA, Perevalov VI. High sensitivity CW-Cavity Ring Down Spectroscopy of N_2O between 6950 and 7653 cm^{-1} (1.44–1.31 μm): II. Line intensities. J Quant Spectrosc Radiat Transfer 2013;117:81–7. doi:10.1016/j.jqsrt.2012.11.003.
7. Liu AW, Kassi S, Perevalov VI, Tashkun SA, Campargue A. High sensitivity CW-cavity ring down spectroscopy of N_2O near 1.28 μm. J Mol Spectrosc 2011;267:191-9. doi:10.1016/j.jms.2011.03.025.
8. Karlovets EV, Kassi S, Tashkun SA, Campargue A. The absorption spectrum of nitrous oxide between 7647 and 7918 cm^{-1}. J Quant Spectrosc Radiat Transfer 2022;288:108199. doi:10.1016/j.jqsrt.2022.108199.
9. Karlovets EV, Campargue A, Kassi S, Perevalov VI, Tashkun SA. High sensitivity Cavity Ring Down Spectroscopy of N_2O near 1.22 μm: (I) Rovibrational assignments and band-by-band analysis. J Quant Spectrosc Radiat Transfer 2016;169:36–48. doi:10.1016/j.jqsrt.2019.02.011.
10. Tashkun SA, Perevalov VI, Karlovets EV, Kassi S, Campargue A. High sensitivity Cavity Ring Down Spectroscopy of N_2O near 1.22 μm: (II) $^{14}N_2{}^{16}O$ line intensity modeling and global fit of $^{14}N_2{}^{18}O$ line positions. J Quant Spectrosc Radiat Transfer 2016;176:62–69. doi:10.1016/j.jqsrt.2016.02.020.
11. Karlovets EV, Kassi S, Tashkun SA, Campargue A. The absorption spectrum of nitrous oxide between 8325 and 8622 cm^{-1}. J Quant Spectrosc Radiat Transfer 2021;262:107508. doi:10.1016/j.jqsrt.2021.107508.
12. Karlovets EV, Tashkun SA, Kassi S, Campargue A. An improved analysis of the N_2O absorption spectrum in the 1.18 μm window. J Quant Spectrosc Radiat Transfer 2022;278:108003. doi:10.1016/j.jqsrt.2021.108003.
13. Gordon IE, Rothman LS, Hargreaves RJ, Hashemi R, Karlovets EV, Skinner FM, Conway EK, Hill C, Kochanov RV, et al. The HITRAN2020 molecular spectroscopic database. J Quant Spectrosc Radiat Transfer 2022;277:107949. doi:10.1016/j.jqsrt.2021.107949.
14. Tashkun SA, Campargue A. The NOSL-296 high resolution $^{14}N_2{}^{16}O$ line list for atmospheric applications. J Quant Spectrosc Radiat Transfer 2023;295:108417. doi:10.1016/j.jqsrt.2022.108417.
15. Toth RA. Linelist of N_2O parameters from 500 to 7500 cm^{-1}, http://mark4sun.jpl.nasa.gov.data/spec/N2O/.
16. Macko P, Romanini D, Mikhailenko SN, Naumenko OV, Kassi S, Jenouvrier A, et al. High sensitivity CW-cavity ring down spectroscopy of water in the region of the 1.5 m atmospheric window. J Mol Spectrosc 2004;227:90–108. doi: 10.1016/j.jms.2004.05.020.

17. Morville J, Romanini D, Kachanov AA, Chenevier M. Two schemes for trace detection using cavity ring down spectroscopy. Appl Phys 2004;D78:465–76. doi: 10.1007/s00340-003-1363-8.
18. Perevalov BV, Kassi S, Romanini D, Perevalov VI, Tashkun SA, Campargue A. CW-cavity ring down spectroscopy of carbon dioxide isotopologues near 1.5 μm. J Mol Spectrosc 2006;238:241–55. doi: 10.1016/j.jms.2006.05.009.
19. Rothman LS, Gordon IE, Barbe A, Chris Benner D, Bernath PF, Birk M, et al. The HITRAN 2008 molecular spectroscopic database. J Quant Spectrosc RadiatTransfer 2009;110:533–72. doi: 10.1016/j.jqsrt.2009.02.013.
20. Tashkun SA. Global modeling of the $^{14}N_2{}^{16}O$ line positions within the framework of the non-polyad model of effective Hamiltonian. J Quant Spectrosc Radiat Transf 2019;231:88–101. doi:10.1016/j.jqsrt.2019.04.023.
21. Tashkun SA, Perevalov VI, Kochanov RV, Liu AW, Hu SM. Global fitting of $^{14}N^{15}N^{16}O$ and $^{15}N^{14}N^{16}O$ vibrational-rotational line positions using the effective Hamiltonian approach. J Quant Spectrosc Radiat Transf 2010;111(9):1089–105. doi: 10.1016/j.jqsrt.2010.01.010.
22. Liu AW, Hu CL, Wang J, Perevalov VI, Hu SM. Cavity ring-down spectroscopy of ^{15}N enriched N_2O near 1.56 μm. J Quant Spectrosc Radiat Transfer 2019;232:1–9. doi: 10.1016/j.jqsrt.2019.04.035.
23. Bertin T, Mondelain D, Karlovets EV, Kassi S, Perevalov VI, Campargue A. High sensitivity cavity ring down spectroscopy of N_2O near 1.74 μm. J Quant Spectrosc Radiat Transf 2019;229:40–9. doi: 10.1016/j.jqsrt.2019.02.011.
24. Toth RA. Line strengths (900-3600 cm^{-1}), self-broadened linewidths, and frequency shifts (1800-2360 cm^{-1}) of N_2O. Applied Optics 1993; 32: 7326-7365. doi: 10.1364/AO.32.007326.
25. Elazizi M, Rachet F, Henry A, Margottin-Maclou M, Valentin A. Linestrength measurements for N_2O around 4 μm: $\Sigma \leftarrow \Sigma$ transitions in four isotopic species (2400-2600 cm^{-1}). J Mol Spectrosc 1994; 164: 180-195. doi: 10.1006/jmsp.1994.1065.
26. Toth RA. Line positions and strengths of N_2O between 3515 and 7800 cm^{-1}. J Mol Spectrosc 1999;197:158–87. doi:10.1006/jmsp.1999.7907.
27. Huang X, Schwenke DW, Lee TJ. Ames-1 296K IR line lists for N_2O isotopologues. In: Proceedings of the The 75th international symposium on molecular spectroscopy, talk TC05; 2022. Available at http://huang.seti.org.

523 **Table 2.** Spectroscopic parameters (in cm^{-1}) for the different bands of N_2O isotopologues assigned in the CRDS spectrum between 7250 and 7653 cm^{-1}.
524

Band [a]	(Pl_2 i)[b]	ΔGv [c]	Gv	Bv	$Dv \times 10^7$	$Hv \times 10^{12}$	RMS [d]	$Nfit/Nobs$ [e]	$Jmax$ $P/Q/R$ [f]	ΔP [g]	Note [h]
$^{14}N_2{}^{16}O$											
3421e-0220e	(14 2 12)	7237.06191(22)	8414.80658(22)	0.41121531(85)	1.3333(83)	-6.28(22)	0.65	75/92	P52/R50	12	1
3421f-0220f		7237.06060(23)	8414.80527(23)	0.41121686(81)	1.2218(77)	1.18(20)	0.70	86/105	P50/R51	12	1
2731e-0330e	(15 3 12)	7241.05404 [i]						/19	R40	12	
2732f-0330f		7241.05416 [i]						/19	R40	12	
3401e-0200e	(14 0 15)	7284.50398(12)	8452.63628(12)	0.40903512(65)	0.3789(79)	6.25(24)	0.54	93/110	P46/R48	12	1
0(14)00e-0200e	(14 0 16)	7307.59339(31)	8475.72569(31)	0.4154876(29)	8.218(67)	55.3(41)	0.66	37/39	P31/R32	12	
0(14)20e-0220e	(14 2 13)	7310.11337(39)	8487.85804(39)	0.4158003(28)	-2.999(48)	-69.2(22)	0.98	39/45	P40/R36	12	
0(14)20f-0220f		7310.11466(29)	8487.85933(29)	0.4158091(10)	3.0303(73)	-	0.73	30/37	P36/R38	12	
5310e-0110e	(13 1 13)	7324.35925(16)	7913.12712(16)	0.41380938(77)	3.1243(88)	7.19(27)	0.56	72/73	P48/R45	12	
5310f-0110f		7324.35825(16)	7913.12612(16)	0.41719121(34)	3.4113(13)	-	0.69	74/75	P54/R50	12	
0512e-0000e	(13 1 4)	7325.61195(29)	7325.61195(29)	0.41110450(95)	2.0622(57)	-	0.64	22/26	P28/R40	13	
0512f-0000e		7325.61265(27)	7325.61265(27)	0.41263612(89)	2.1256(53)	-	0.62	21/23	Q42	13	
6200e-1000e	(14 0 17)	7328.04505(29)	8612.94839(29)	0.4131284(14)	4.978(16)	19.33(51)	0.64	36/41	P44/R46	12	
5200e-0000e	(12 0 13)	7340.791714(98)	7340.791714(98)	0.41527767(37)	5.3702(31)	25.066(67)	0.45	94/97	P57/R56	12	
5220e-0000e	(12 2 10)	7355.03464(95)	7355.03464(95)	0.4157264(22)	-0.662(16)	-25.14(33)	0.76	39/46	P53/R55	12	
0114e-1110e	(17 1 1)	7365.81705(32)	9246.08279(32)	0.40553414(83)	1.7836(43)	-	0.61	21/33	P45/R40	14	
0114f-1110f		7365.81784(37)	9246.08358(37)	0.4062805(14)	1.8153(90)	-	0.80	17/24	P40/R39	14	
0004e-1000e	(16 0 1)	7429.23729(11)	8714.14063(11)	0.40518474(31)	1.7741(15)	-	0.53	81/85	P48/R47	14	
7110e-1110e	(15 1 18)	7430.65489(29)	9310.92063(29)	0.4098825(13)	2.266(11)	-	0.57	23/27	P36/R31	12	
7110f-1110f		7430.65576(46)	9310.92150(46)	0.4128955(22)	2.273(18)	-	0.74	14/16	P34/R33	12	
7110e-0310e	(15 1 17)	7436.63295(60)	9185.69818(60)	0.4115991(28)	2.897(26)	-	0.69	15/19	P32/R29	13	
7110f-0310f		7436.63275(73)	9185.69790(73)	0.4151885(29)	3.307(21)	-	0.72	9/11	P26/R34	13	
7000e-1000e	(14 0 18)	7440.19671(13)	8725.10005(13)	0.41049861(66)	3.0211(73)	8.74(21)	0.52	81/87	P49/R50	12	
2112e-0000e	(13 1 7)	7443.00813(34)	7443.00813(34)	0.4089097(16)	1.039(16)	-10.18(36)	0.65	18/53	P45/R53	13	2
2112f-0000e		7443.00360(86)	7443.00360(86)	0.4099529(18)	1.286(10)	-	0.67	8/26	Q42	13	
6200e-0200e	(14 0 17)	7444.81579(20)	8612.94809(20)	0.4131324(10)	5.035(13)	21.26(39)	0.60	56/60	P48/R45	12	
6220e-0220e	(14 2 14)	7453.38703(27)	8631.13170(27)	0.4138709(15)	-0.237(21)	-19.65(75)	0.75	49/51	P43/R43	12	
6220f-0220f		7453.38851(21)	8631.13318(21)	0.41386573(60)	2.2853(34)	-	0.75	48/58	P46/R41	12	
6220f-0220e								4/5	Q09	12	
0403e-1000e	(16 0 2)	7454.439982(54)	8739.30316(54)	0.4106908(28)	3.817(26)	-	0.95	17/20	P27/R32	14	

6110e-0110e	(13 1 14)	7457.58225(12)	8046.35012(12)	0.41192828(44)	2.4229(38)	3.262(87)	0.49	90/94	P57/R53	12	
6110e-0110f								4/9	Q16	12	
6110f-0110f		7457.58177(11)	8046.34964(11)	0.41473850(41)	2.5632(33)	2.439(67)	0.52	88/94	P59/R58	12	
6110f-0110e								7/7	Q21	12	
6000e-0000e	(12 0 14)	7463.98523(11)	7463.98523(11)	0.41279933(27)	3.2651(15)	7.080(22)	0.56	123/135	P71/R70	12	3
5220e-0000e	(12 2 11)	7488.62925(53)	7488.62925(53)	0.4140536(11)	0.8974(61)	-9.26(10)	0.65	54/65	P63/R61	12	
0114e-0310e	(17 1 1)	7497.01312(59)	9246.07835(59)	0.4055641(43)	2.146(53)	-	0.84	12/15	P27/R27	14	
0114f-0310f		7497.01677(64)	9246.08192(64)	0.4062965(38)	1.976(35)	-	0.82	14/18	P31/R30	14	
0533e-0330e	(17 3 3)	7522.09826(32)	9289.01065(32)	0.4114482(20)	1.516(25)	-	0.60	29/32	P28/R26	14	
0533f-0330f		7522.09834(31)	9289.01058(31)	0.4114513(20)	1.537(25)	-	0.59	29/32	P28/R26	14	
6200e-1000e	(14 0 19)	7525.86136(27)	8810.76470(27)	0.4094690(28)	0.627(25)	9.90(57)	0.78	24/87	P46/R52	12	4
0513e-0310e	(17 1 2)	7526.07994(44)	9275.14517(44)	0.4100991(20)	2.368(15)	-	0.70	18/24	P36/R26	14	
0513f-0310f		7526.07724(37)	9275.14239(37)	0.4121525(14)	2.737(11)	-	0.66	22/27	P33/R35	14	
0004e-0200e	(16 0 1)	7546.00813(17)	8714.14043(17)	0.40518536(51)	1.7769(28)	-	0.67	57/69	P45/R45	14	
6000e-0000e	(12 0 15)	7556.135163(88)	7556.135163(88)	0.41065810(31)	1.6107(25)	7.501(52)	0.42	113/114	P58/R57	12	
7000e-0200e	(14 0 18)	7556.96979(30)	8725.10209(30)	0.41048250(99)	2.7817(58)	-	0.89	37/45	P43/R35	12	
0423e-0220e	(16 2 1)	7568.84589(15)	8746.59056(15)	0.41087041(76)	0.1084(87)	-16.76(26)	0.59	58/63	P51/R40	14	
0423e-0220f								5/5	Q08	14	
0423f-0220f		7568.84639(13)	8746.59106(13)	0.41087048(36)	2.1331(17)	-	0.58	57/64	P50/R42	14	
0423f-0220e								5/5	Q08	14	
6110e-0110e	(13 1 15)	7570.89543(25)	8159.66330(25)	0.4106216(19)	1.566(14)	2.70(27)	0.78	31/119	P58/R58	12	5
6110f-0110f		7570.89374(16)	8159.66161(16)	0.4130766(14)	1.789(17)	34.81(55)	0.52	48/90	P46/R45	12	
0403e-0200e	(16 0 2)	7571.17235(18)	8739.30465(18)	0.41069182(81)	3.9995(84)	16.97(22)	0.62	65/75	P56/R52	14	
5420e-0220e	(14 2 15)	7582.34992(29)	8760.09459(29)	0.4125766(15)	1.274(20)	-10.17(66)	0.82	46/56	P36/R45	12	
5420e-0220f								3/3	Q06	12	
5420f-0220f		7582.34948(30)	8760.09415(30)	0.4125778(17)	1.632(22)	4.36(74)	0.84	39/50	P38/R45	12	
5420f-0220e								3/3	Q06	12	
0911e-0000e	(13 1 8)	7589.42023(80)	7589.42023(80)	0.4130956(48)	5.155(77)	8.19(35)	0.62	17/22	R36	13	
0911f-0000e		7589.4243(15)	7589.4243(15)	0.4155234(91)	5.29(10)	-		3/5	Q27	13	
1203e-1000e	(16 0 4)	7592.13856(29)	8877.04189(29)	0.4079641(12)	2.3436(98)	-	0.60	18/24	P26/R36	14	
3620e-0000e	(12 2 12)	7610.6169(28)	7610.6169(28)	0.4134111(56)	1.709(33)	-8.70(61)	0.57	20/25	P46/R53	12	
0313e-0110e	(15 1 1)	7616.50056(10)	8205.26843(10)	0.40960363(33)	2.0982(25)	1.129(48)	0.49	94/100	P63/R58	14	
0313e-0110f								10/10	Q13	14	
0313f-0110f		7616.500136(93)	8205.268006(93)	0.41102324(20)	2.19690(79)	-	0.52	86/92	P53/R55	14	

0313f-0110e								12/16	Q22	14	
4600e-1000e	(14 0 20)	7621.71108(30)	8906.61442(30)	0.4113021(13)	-1.267(11)	-	0.83	31/34	P33/R36	14	
0623e-0420e	(18 2 4)	7634.70063(47)	9965.82214(47)	0.4090960(25)	0.826(22)	-	0.67	14/17	P20/R31	14	
1443e-0440e	(18 4 12)	7637.13944(50)	9993.39186(50)	0.4098035(19)	1.653(15)	-	0.65	17/20	P27/R33	14	
3600e-0000e	(12 0 16)	7640.47386(11)	7640.47386(11)	0.41185011(39)	-0.0798(32)	8.863(69)	0.50	112/114	P56/R57	12	6
2113e-1110e	(17 1 7)	7657.00168(53)	9537.26742(53)	0.4055794(36)	1.711(20)	-	0.88	14/40	P42/R27	14	6,7
2113f-1110f		7657.00042(67)	9537.26416(67)	0.4066022(84)	1.12(22)	-	0.75	11/30	P38/23	14	
1004e-0001e	(18 0 4)	7664.81080(48)	9888.56757(48)	0.4033296(35)	1.461(57)	-10.4(19)	0.69	20/40	P47/R28	14	6,8
0203e-0000e	(14 0 1)	7665.273348(86)	7665.273348(86)	0.40978360(26)	2.5061(17)	3.448(31)	0.44	122/125	P64/R63	14	6
0223e-0000e	(14 2 1)	7673.63709(64)	7673.63709(64)	0.4099805(15)	1.1548(99)	-3.54(19)	0.76	56/63	P59/R52	14	6
1333e-0330e	(17 3 3)	7674.09722(19)	9441.00960(19)	0.40909436(43)	1.5884(18)	-	0.63	53/58	P51/R44	14	6
1333f-0330f		7674.09763(34)	9441.00987(34)	0.4090959(12)	1.625(12)	3.53(32)	0.65	45/48	P51/R41	14	6
3710e-0110e	(13 1 16)	7677.51544(20)	8266.28331(20)	0.41080657(98)	1.024(12)	6.42(36)	0.65	67/76	P49/R41	12	6
3710f-0110f		7677.51602(19)	8266.28389(19)	0.41338623(99)	0.371(13)	2.67(44)	0.64	71/78	P46/R44	12	6
2003e-1000e	(16 0 7)	7691.58474(18)	8976.48808(18)	0.40513676(94)	1.6902(75)	2.99(16)	0.73	57/98	P59/R51	14	6,9
1203e-0200e	(16 0 4)	7708.90881(12)	8877.04111(12)	0.40796932(44)	2.4140(35)	2.953(76)	0.53	94/101	P58/R56	14	6
1223e-0220e	(16 2 3)	7710.77485(15)	8888.51952(15)	0.40837749(72)	1.2477(45)	-2.095(75)	0.56	44/94	P53/R62	14	6,10
1223f-0220f		7710.77513(11)	8888.51980(11)	0.40837379(36)	1.79191(88)	-	0.42	41/98	P57/R62	14	
1113e-0110e	(15 1 3)	7747.02838(12)	8335.79625(12)	0.40719885(27)	1.7219(14)	0.222(19)	0.51	107/119	P74/R65	14	6
1113f-0110f		7747.02832(11)	8335.79619(11)	0.40804222(26)	1.7036(13)	0.353(18)	0.48	113/126	P73/R68	14	6
$^{14}N^{15}N^{16}O$											
5200e-0000e	(12 0 14)	7384.07735(36)	7384.07735(36)	0.4129979(18)	4.404(22)	19.42(69)	0.70	26/33	P32/R46	12	
6000e-0000e	(12 0 15)	7492.12185(17)	7492.12185(17)	0.41043674(59)	2.3639(38)	-	0.67	56/63	P42/R41	12	
0203e-0000e	(14 0 1)	7511.63701(21)	7511.63701(21)	0.4101381(14)	2.842(20)	6.63(75)	0.60	43/52	P42/R43	14	
5200e-0000e	(12 0 16)	7567.42932(24)	7567.42932(24)	0.40922107(89)	0.6800(64)	-	0.72	37/43	P40/R35	12	
1113e-0110e	(15 1 3)	7614.99808(16)	8190.43173(16)	0.40740129(50)	1.7501(27)	-	0.58	46/54	P46/R43	14	
1113e-0110f								2/4	Q06	14	
1113f-0110f		7614.99849(19)	8190.43214(19)	0.40822660(58)	1.7286(32)	-	0.68	47/57	P46/R41	14	
1113f-0110e								2/2	Q03	14	
1003e-0000e	(14 0 3)	7650.753947(89)	7650.753947(89)	0.40710109(19)	1.72924(73)	-	0.48	93/100	P57/R51	14	6
$^{15}N^{14}N^{16}O$											
5200e-0000e	(12 0 13)	7275.89874(28)	7275.89874(28)	0.4013148(20)	4.375(35)	6.16(16)	0.60	29/37	P28/R38	12	
6000e-0000e	(12 0 14)	7394.27113(14)	7394.27113(14)	0.39887412(75)	2.7847(88)	5.50(28)	0.51	60/63	P42/R47	12	
6000e-0000e	(12 0 15)	7482.85458(19)	7482.85458(19)	0.39745044(98)	1.075(12)	7.32(41)	0.53	54/65	P43/R45	12	
0313e-0110e	(15 1 1)	7543.00758(76)	8128.31970(76)	0.3956707(38)	1.776(34)	-	0.71	9/16	P33/R28	14	

0313f-0110f		7543.00305(64)	8128.31517(64)	0.3970185(28)	2.184(26)	-	0.73	16/20	P33/R26	14	
0203e-0000e	(14 0 1)	7592.48553(20)	7592.48553(20)	0.39584295(90)	2.2379(97)	2.18(28)	0.63	58/65	P48/R49	14	
1203e-0200e	(16 0 4)	7629.70073(67)	8789.67244(67)	0.3941395(29)	2.109(21)	-	0.69	11/16	P22/R33	14	
1113e-0110e	(15 1 3)	7667.80648(36)	8253.11860(36)	0.3934939(12)	1.5783(65)	-	0.82	28/45	P44/R27	14	6
1113f-0110f		7667.80474(35)	8253.11686(35)	0.3943209(26)	1.923(45)	14.1(21)	0.74	29/49	P40/R28	14	6
1003e-0000e	(14 0 3)	7702.49927(11)	7702.49927(11)	0.39310930(37)	1.5910(26)	0.660(48)	0.53	95/101	P64/R59	14	6
$^{14}N_2{}^{16}O$											
6000e-0000e	(12 0 14)	7292.37397(14)	7292.37397(14)	0.38920233(72)	2.2164(85)	6.11(26)	0.47	59/63	P40/R47	12	
5200e-0000e	(12 0 15)	7376.57120(22)	7376.57120(22)	0.38938671(94)	0.1517(70)	-	0.69	39/42	P37/R37	12	
0203e-0000e	(14 0 1)	7630.84269(17)	7630.84269(17)	0.38684019(45)	2.1569(22)	-	0.66	55/63	P50/R40	14	
1003e-0000e	(14 0 3)	7718.94756(11)	7718.94756(11)	0.38434089(38)	1.4574(30)	0.536(61)	0.47	90/99	P57/R58	14	6

Notes

The confidence interval (1SD) is in the units of the last quoted digit.

[a] $V_1V_2l_2V_3$ correspond to the maximum value of the modulo of the expansion coefficients of the eigenfunction. V_2 is given between parenthesis when it is larger than 10. Bold characters are used for the newly assigned bands,

[b] Cluster labeling notation: ($P= 2V_1+V_2+4V_3$, l_2, i), i is the order number within the cluster increasing with the energy. We correct here a ten of erroneous values of the i ranking number given in Ref. [5],

[c] $G_v=G_v^{'}-G_v^{''}$ is the band center,

[d] Root Mean Square of the (Obs.-Calc.) differences of the position values (in 10^{-3} cm^{-1} unit),

[e] N_{fit} is the total number of transitions included in the fit; N_{obs} is the total number of measured transitions of the considered band,

[f] Observed branch with the maximum value of the total angular momentum quantum number of the input data,

[g] $P=P'-P''$, where P' and P'' are the upper and lower polyads.

[h] Notes

1 – Line positions from Ref. [5] were included in the fit;

2 – Anharmonic resonance (13 1 7) ↔ (13 1 6) (J_{cross}= 17);

3 – Intrapolyad Coriolis resonance (12 0 14) ↔ (12 3 5) (J_{cross}= 36);

4 –Interpolyad anharmonic (14 0 19) ↔ (16 0 3) (J_{cross}= 24);

5 –Three interpolyad Coriolis resonances (13 1 15) ↔ (14 2 6) (J_{cross} = 27); (13 1 15) ↔ (14 2 9) (J_{cross} = *e*: 17 and *f:* 21) and (13 1 15) ↔ (14 0 11) (J_{cross} =37);

6 – Line positions from Ref. [8] were included in the fit;

7 – Interpolyad anharmonic resonance (17 1 7) ↔ (15 1 11) (J_{cross} =31);

8 – Intrapolyad anharmonic resonance (18 0 4) ↔ (18 0 3) (J_{cross} =13) and Interpolyad Coriolis resonance (18 0 4) ↔ (17 1 10) (J_{cross}=35);

9 - Intrapolyad anharmonic (16 0 7) ↔ (16 0 6) (J_{cross}= 32);

10 - Interpolyad Coriolis resonance (16 2 3) ↔ (15 1 13) (J_{cross}= *e*: 32, J_{cross}= *f*: 32);

[i] Band center provided by the global effective Hamiltonian.

548